Proc. of IEEE ISPLC 2013

PLC Noise and Channel Characterization in a Compact Electrical Car

Massimo Antoniali, Marco De Piante, and Andrea M. Tonello
WiPLi Lab - Università di Udine - Via delle Scienze 208 - 33100 Udine - Italy
e-mail: massimo.antoniali@uniud.it, marco.depiante@uniud.it, tonello@uniud.it

***Abstract*—The use of power line communications (PLC) for the interconnection of devices inside vehicles is interesting because it can provide cost and weight reduction of the wiring harness. However, despite the compact size of the in-car electrical grid, high channel attenuation, low impedance access points, and high noise can limit the applicability of PLC. In this paper we report the results of a measurement campaign in a compact electrical car. We focus on the noise and channel response both in the narrow band range (30-500 kHz) and broad band range (2-100 MHz). We show that the electrical power drivers and DC/DC converters on board cause high noise which is more pronounced at low frequencies. Achievable rate analysis shows that the broad band spectrum is more suited for in-car PLC communications.**

I. Introduction

New generation vehicles deploy a wide set of sensors and electronic equipment. To interconnect them, power line communication (PLC) is an attractive solution. Since PLC exploits the existing power infrastructure to deliver data services, it is a candidate telecommunication technology for the future smart cars.

Focusing on the electrical vehicles, PLC is an interesting solution also due to the intrinsic nature of the electric power system, with respect to the wiring infrastructure of standard vehicles. In fact, electrical vehicles are equipped with a dedicated power grid to supply the electric engine. Battery management to control charge, discharge and energy flow to the electric engine and electronic equipment can be made by integrated boards and electronic control units (ECUs) connected via power cables. The benefits of using PLC are the reduction of weight, cost and complexity of the vehicle wiring harness.

Early works deal with the analysis of the potentiality of in-vehicle PLC in conventional cars [1]-[12]. The electrical vehicle scenario has not been deeply investigated yet. The PLC channel characterization in a fully electric commercial vehicle is the topic of the research activity in [13]. In [14], the authors focus on a hybrid electrical vehicle and present the results of a PLC channel measurement campaign.

In this paper, we report the results of the experimental power line measurement campaign that we have carried out in a 4-wheel compact electrical car. We study the impact of the existing electric and electronic systems on the PLC transmission medium, and we dig into the noise generated by such devices. We address both the narrow band (NB) and the broad band (BB) frequency range. Herein, we investigate the data transmission performance in terms of theoretical achievable rate.

The work of this paper has been supported in part by the Friuli Venezia Giulia Region under the project LR 14/2010 art. 16 ESTAMOS (Electronics and Systems in the Electrical Car for Sustainable Mobility), http://www.progettoestamos.it.

Fig. 1. Measurement scenario with the electrical vehicle under test.

The paper is organized as follows. Section II provides and overview of the vehicle under test. Section III explains the measurement scenario and setup. In Section IV, we provide the full set of results, i.e., noise, channel, and impedance results. In the NB, we also provide an analytic expression for the harmonic content of the PLC noise that we have measured. Section V addresses the results of the theoretical analysis of the potential data transmission performance. Finally, some conclusions follow.

II. Overview of the Vehicle Under Test

We have performed the power line measurement campaign over the electric power system of the Birò [15] which is a 4-wheel compact electrical car made in Italy. The vehicle under test, shown in Fig. 1, is equipped with two 3-phases brushless 48V electric engines. Each electric engine moves one of the two rear wheels. Power is ensured by a battery pack that comprises four 12V-100Ah lead gel batteries. The battery pack directly supplies the two ECUs that drive the electric engines. Basically, each ECU controls the flow of the current through the three coils of the engine, i.e, the three phases. The rotation of the rotor of the electric engine is ensured by the commutation of the power through the three phases according to a certain control sequence. A DC/DC converter is used to convert 48V DC to 12V DC, in order to supply the 12V power network of the vehicle. The 12V electrical system feeds the 12V standard peripherals, i.e., lights, break lights, turn lights. The 12V output of the DC/DC converter feeds

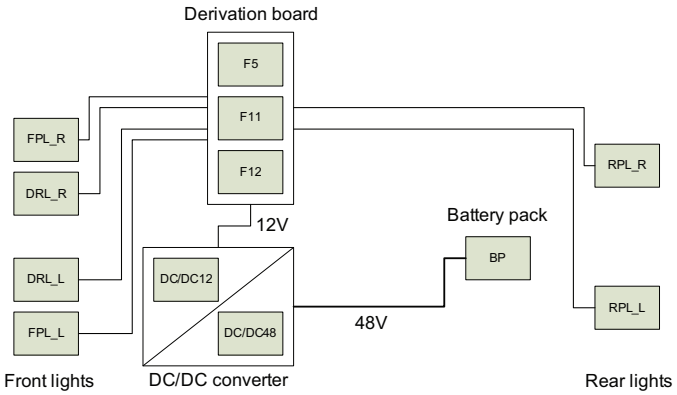

Fig. 2. Schematic of the measurement scenario.

TABLE I
LIST OF THE TEST POINTS

Test Point	Acronym
Front position light, left	FPL_L
Daytime running light, left	DRL_L
Front position light, right	FPL_R
Daytime running light, right	DRL_R
Rear position light, left	RPL_L
Rear position light, right	RPL_R
Battery pack (48V terminals)	BP
DC/DC converter (48V side)	DC/DC48
DC/DC converter (12V side)	DC/DC12
Fuse brake lights	F5
Fuse FPL_L-RPL_R	F11
Fuse FPL_R-RPL_L	F12

a derivation board. All the 12V peripherals are connected to the derivation board through two feeding conductors. Groups of nearby devices share the same negative wire. The negative wire is distributed to all nodes from the negative pole of the battery and it is not connected to the chassis.

III. Measurement Scenario and Setup

We have selected a set of strategic access points for PLC purposes. In the 12V power network, we have placed test points in proximity of the front position and daytime running lights, the rear position lights, in the derivation board (fuse box) and the DC/DC converter (12V side). In the 48V electric power system, we have focused on the battery pack and the DC/DC converter (48V side). The test points can resemble hypothetical PLC nodes, i.e., sensors or new generation lighting drivers controlled via power cables. Fig. 2 depicts the schematic of the measurement scenario. In detail, the DC/DC converter is physically located in the front part of the vehicle, near the derivation board. This fact has a strong impact on PLC channel measurements, as it will be explained in the following. We have placed test connectors in parallel to the feeding conductors of the peripherals, without disconnecting them from the power supply grid. In the fuse box, we have replaced the correspondent fuse with a built-in connector that acts as a shunt connector but, at the same time, it allows access to the test node. The physical length of the connectors does not affect the PLC channel properties.

To ease the notation, in the following, we use the acronyms of Table I to denote the test points.

We have performed measurements both in the NB and BB frequency range. We have deployed NB and BB capacitive couplers to protect the measurement equipment from the power supply voltage. The frequency response of the NB couplers is flat in the frequency range 3-500 kHz. The BB couplers allow reliable measures up to 100 MHz.

Noise measurements have been made in the time domain using a digital storage oscilloscope (DSO) with a 50 Ω input impedance adapter. The DSO has been auto-triggered. From the noise samples, we have obtained the power spectral density (PSD) of the PLC noise via a periodogram. The sampling rate, the time window and the memory depth of the DSO have been fixed according to the desired time span, frequency range and resolution. In detail, for NB noise measures, we have collected 100k samples with a sampling rate equal to 50 MSamples/s (Δf=500 Hz). For the BB case, we have collected 1M points per trace, with rate of 250 MSamples/s (Δf=250 Hz).

The channel and impedance measurements have been performed in the frequency domain using a vector network analyzer (VNA). We limited the number of access points for the channel and impedance measurements. In fact, we have experienced high level of background noise on the test points in proximity of the DC/DC converter (both 48V and 12V side) and in the derivation board. To prevent the damage of the VNA, we discarded the aforementioned test points. The VNA has been set to acquire 1601 points in the NB and BB frequency range of 3-500 kHz and of 2-100 MHz.

Basically, we have performed the noise and channel measurements for three different states of the vehicle, i.e., a) electric engines OFF: the front and rear position lights and the daytime running lights are switched ON but the electric engines are in idle state, b) electric engines ON: the electric engines are running but not under heavy load condition, c) the same as in b) but in heavy load condition.

IV. Measurement Results

In the following, we first analyze the PLC noise, within the NB and BB frequency range. In the NB, we provide an analytic expression for the harmonic noise components. Then, we present the channel and impedance measurement results.

A. PLC Noise

Firstly, we present the results of the noise measurements in the NB frequency range, with a description of the noise components. Afterwards, we will present the results for the BB spectrum. In this particular PLC environment, the main noise source is the DC/DC converter. As we have described in the previous sections, this block allows to feed the 12V peripherals with the 48V available voltage. The switching DC/DC converter comprises two reactive components, typically an inductor and a capacitor connected as a LC lowpass

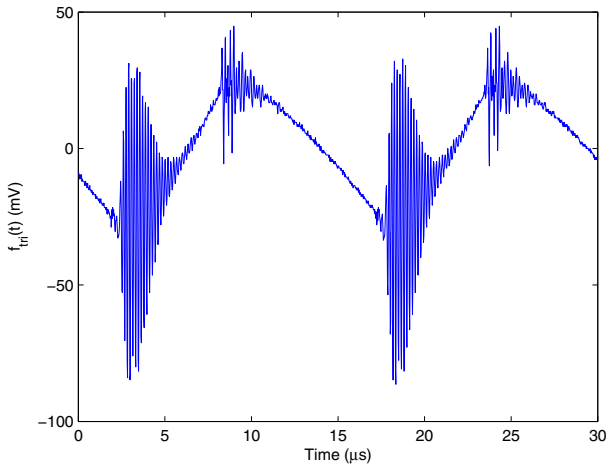

Fig. 3. Noise voltage waveform experienced at the DRL_L access point. The electric engines were running under heavy load condition.

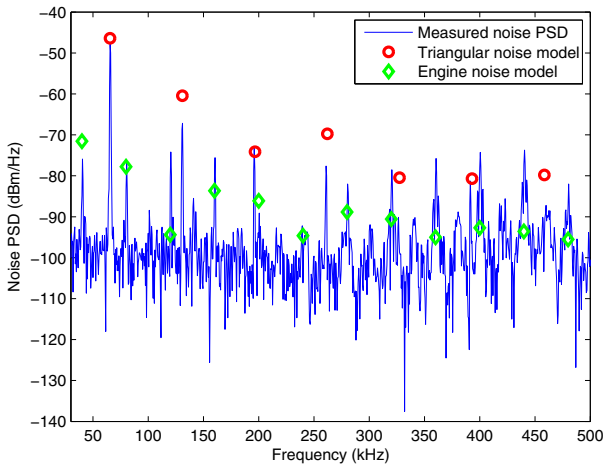

Fig. 5. PSD of the NB noise experienced at the DRL_L access point. The electric engines were running under heavy load condition.

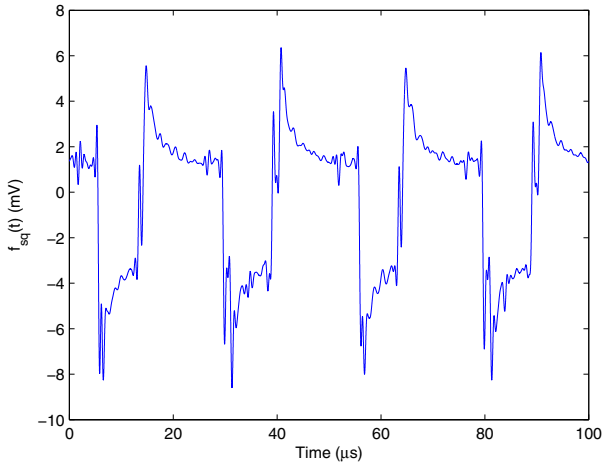

Fig. 4. Squared power engine waveform measured on a solenoid wrapped on a phase of one of the two engines.

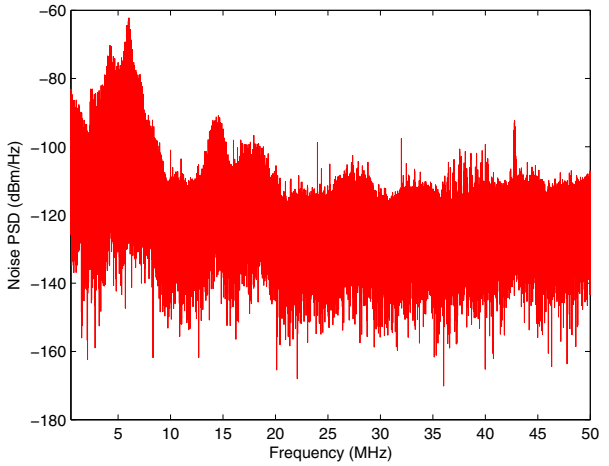

Fig. 6. PSD of the BB noise experienced at the DRL_L access point. The electric engines were running.

filter, a MOSFET used as a switch and a diode. The MOSFET is driven with a square wave with a specified duty cycle that gives the conversion ratio. When the square wave is high, the input voltage charges the inductor and the diode is turned OFF. Viceversa, with a low level of the square wave, the diode is turned ON with the discharge current of the inductor. The result at the output is a constant voltage with a triangular ripple caused by the charge-discharge cycle on the inductor. For this reason, the measured noise is composed by a triangular waveform with an additional resonance effect that introduces a high frequency contribution for the noise. The resonance is caused by the reactive components inside the DC/DC converter. Since the MOSFET active transistor is driven by a square wave as mentioned above, this causes a discontinuous current flow to the LC low-pass filter. At the falling or rising edges of the square wave, a overshooting response is added to the triangular ripple voltage. This particular waveform is the common ripple signal present at the output of a switching converter. In the following we will refer to it as triangular noise. To measure the noise we have used a DSO. Fig. 3 shows the triangular waveform measured at the DRL_L access point. Here, the overshooting is limited to a small voltage value, and the dynamic voltage range of the DSO is entirely used to acquire the noise signal with the best accuracy. We can notice the superposition of another noise component that is present when the engine is in high load condition. It is possible to derive an analytic expression for the triangular noise signal that affects the NB spectrum as follows:

$$\begin{cases} f_{tri}^{(1)}(t) = A_{tri}\left(\frac{1}{D_{DC}\cdot T_{DC}}t - 1\right); & t \in [0, D_{DC}T_{DC}[\\ f_{tri}^{(2)}(t) = \frac{A_{tri}}{1-D_{DC}}(1+D_{DC}) - \\ \qquad\qquad + \frac{A_{tri}}{1-D_{DC}}\frac{1}{T_{DC}}t; & t \in [D_{DC}T_{DC}, T_{DC}] \end{cases} \quad (1)$$

where T_{DC}, A_{tri}, and D_{DC} are respectively the period, the amplitude and the duty cycle of the triangular waveform. Particularly, the duty cycle depends on the duty cycle of the square waveform that drives the MOSFET transistor. With the Fourier expansion series, it is possible to describe analytically the occupied spectrum:

$$f_{tri}(t) \sim \sum_{k=1}^{+\infty} a_k^{(tri)} \cos\left(\frac{2\pi t}{T_{DC}}k\right) + b_k^{(tri)} \sin\left(\frac{2\pi t}{T_{DC}}k\right) \quad (2)$$

with

$$\begin{cases} a_k^{(tri)} = \frac{A_{tri}}{(k\pi)^2}\left[\frac{1}{D_{DC}}[\cos(2\pi k D_{DC}) - 1] + \right. \\ \qquad \left. - \frac{1}{1-D_{DC}}[1 - \cos(2\pi k D_{DC})]\right] \\ b_k^{(tri)} = \frac{A_{tri}\sin(2\pi k D_{DC})}{\pi^2 k^2 D_{DC}(1-D_{DC})}. \end{cases} \quad (3)$$

The triangular noise has a period of $T_{DC} \approx 15.4\ \mu s$, with a duty cycle $D_{DC} \approx 0.37$. This suggests that a fly-back DC/DC converter has been used.

Another noise source is given by the power signal that feeds the engines. The loaded engine requests a great amount of current to move the wheels, and the current that drives the engines is composed of a square waveform with a different duty cycle D_{EN} for each of the three phases. Fig. 4 depicts the square waveform measured on a solenoid wrapped on a phase wire of one of the two engines. This current generates a magnetic field that is concatenated with the rest of the electrical power system. This induces a noise voltage on the other wires, that depends to the load at the engines with an amplitude A_{sq}. This value depends on the amount of current requested by the engines. The Fourier expansion series for the engines' concatenated voltage is

$$f_{sq}(t) \sim \sum_{k=1}^{+\infty} a_k^{(sq)} \cos\left(\frac{2\pi t}{T_{EN}}k\right) + b_k^{(sq)} \sin\left(\frac{2\pi t}{T_{EN}}k\right) \quad (4)$$

with

$$\begin{cases} a_k^{(sq)} = \frac{A_{sq}}{k\pi}\sin(2\pi k D_{EN}) \\ b_k^{(sq)} = \frac{A_{sq}}{k\pi}[1 - \cos(2\pi k D_{EN})]. \end{cases} \quad (5)$$

For the engines' current, we have calculated $T_{EN} \approx 25\ \mu s$ and $D_{EN} \approx 0.67$.

In the NB, all the harmonic components have been analytically calculated. The measured spectrum is shown in Fig. 5 when the electric engines are under heavy load conditions. As it should be noticed, the highest harmonics are multiple of $1/T_{DC}$, i.e. 65 kHz. The loaded engines instead cause a lot of harmonic contributions at the multiple frequencies of $1/T_{EN}$, i.e., 40 kHz.

Now, the BB measurements allows us to explore the PSD of the noise at frequencies above 500 kHz. The main contribution is given by the overshooting oscillations. Measuring the oscillation period, we have found a spectral occupancy in the range of 4.5-6.5 MHz. In Fig. 6, we show the measured PSD up to 25 MHz. For higher frequencies, the measured PSD approaches the noise floor of the DSO.

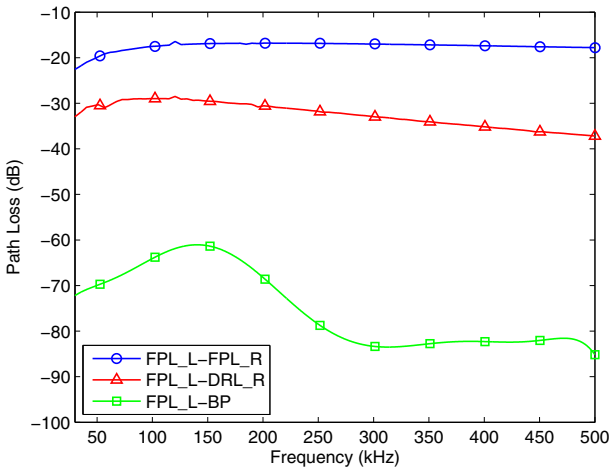

Fig. 7. NB path loss of the three representative channels, i.e., one for each of the three classes.

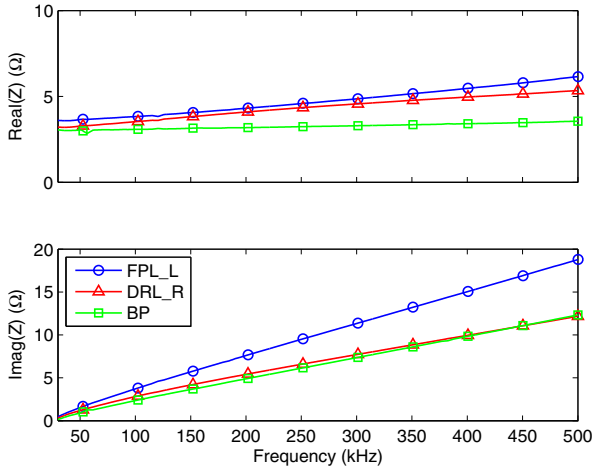

Fig. 8. NB access impedance of the three representative test points.

B. PLC Channel and Impedance

Herein, we provide results in terms of path loss, i.e., $PL(f) = |H(f)|^2$, where $H(f)$ is the channel transfer function (CTF) between two test points. Firslty, we classify the channels into three different classes, according to their NB path loss profile. In Fig. 7, we show the path loss of three representative channels, i.e., one for each of the three classes. In the NB, we have not experienced substantial differences between the channel frequency response for the three different states of the vehicle. Furthermore, there is no relation between the physical length of the electrical paths and the attenuation profiles. We note that the most attenuated channels are the power links between the BP and the other access points. This is amenable to the presence of the DC/DC converter that blocks the NB PLC signal.

In Fig. 8, we analyze the access impedance for three different access points, i.e., in proximity of the FPL_L, the DRL_L and the BP. From measures, we have found that both

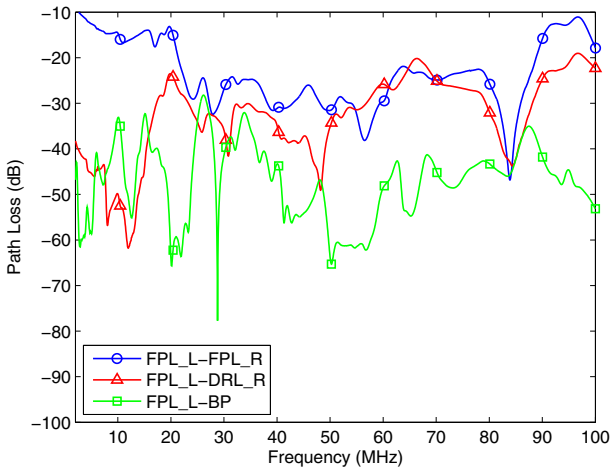

Fig. 9. BB path loss of the three representative channels, i.e., the same channels of Fig. 7.

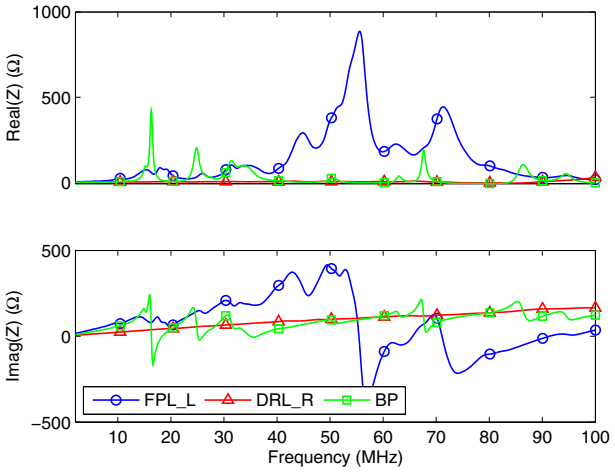

Fig. 10. BB access impedance of the three representative test points, i.e., the same access points of Fig. 8.

the light bulbs and the battery pack impose a low impedance value to the access impedance. The imaginary part of the impedance shows an inductive behavior in the frequencies of interest, due to the fact that a light bulb is basically composed by a coil of metal wire. The very low impedance values of the aforementioned loads are also the cause of the high attenuation of the PLC channel. Thus, we also investigate the channel frequency response in the 2-100 MHz band. The purpose is to evaluate the possibility to convey BB PLC signal through the power cables of the vehicle under test. Fig. 9 and Fig. 10 show respectively the path loss and the access impedance profiles of the same links of Figs. 7-8.

V. Data Transmission Performance

From measures, we study the potential data transmission performance in terms of theoretical achievable rate, in the NB and BB frequency range. In the NB, we focus on the Cenelec bands A, B, and C. In the BB, we focus on the HPAV

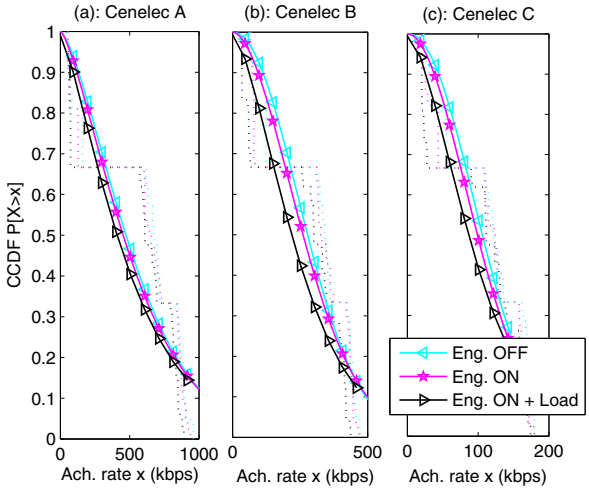

Fig. 11. CCDF of the theoretical link achievable rate in the Cenelec bands A (a), B (b), and C (c).

frequency band 2-28 MHz [16] and in the extended band 2-100 MHz. The theoretical achievable rate C, under the additive Gaussian noise assumption, reads as follows

$$C = \Delta f \sum_{m=1}^{M} \log_2 \left(1 + \frac{P_{tx}(f_m)|H(f_m)|^2}{P_w(f_m)} \right) [bps], \qquad (6)$$

where $P_{tx}(f_m)$ and $P_w(f_m)$ are respectively the PSD of the transmitted signal and the PSD of the measured noise at frequency f_m, M is the number of sub-carriers and Δf is the sub-carrier frequency spacing. The parameters in (6) are reported in Table II, respectively for the NB and BB cases. In both situations, we assume the PSD of the transmitted signal to be constant.

In Fig. 11, we show the complementary distribution function (CCDF) of the achievable rate for the Cenelec bands A, B, and C, for the three different states of the vehicle. As shown in subplot (a), the 70-th percentile of the CCDF correspondent to the Cenelec band A is in excess of 240 kbps and up to 300 kbps, respectively for the turned OFF engines case and heavy loaded engines case. Similarly, in the Cenelec band B, the depicted CCDF shows that the theoretical rate is in excess of 140 kbps and up to 200 kbps, respectively for the turned OFF engines case and heavy loaded engines case. In the Cenelec band C, the theoretical achievable rate is in excess of 60 kbps and up to 80 kbps. It should be noticed that the maximum achievable data rate decreases when we move from Cenelec A to Cenelec C. This is caused by the decrease of the bandwidth assigned to the three mentioned standard bands.

Although not reported for space limitations, we have experimentally investigated the performance of NB-PLC devices operating in the Cenelec bands A, B, C that implement the main G3-PLC [17] specifications. On average, the experimental data rates are 90-98% lower than the one ones predicted theoretically. This makes us think that it is necessary to appropriately change/adapt the G3-PLC specifications to obtain a valid and robust solution for the in-vehicle scenario.

TABLE II
PARAMETERS FOR NB AND BB DATA TRANSMISSION PERFORMANCE ANALYSIS.

Parameter	Cenelec A	Cenelec B	Cenelec C	HPAV	HPAV Ext.
Start frequency	35.938 kHz	98.4375 kHz	128.125 kHz	2 MHz	2 MHz
Stop frequency	90.625 kHz	121.875 kHz	137.500 kHz	28 MHz	100 MHz
Δf (kHz)	1.5625	1.5625	1.5625	24.414	24.414
M	36	16	7	1065	4015
P_{tx} (dBm/Hz)	-30	-30	-30	-50	-50

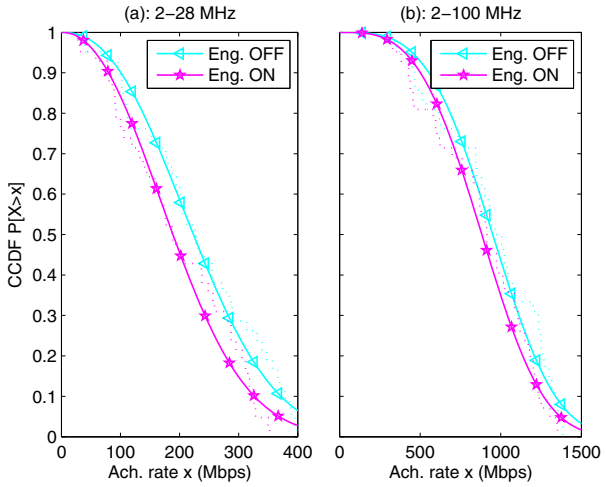

Fig. 12. CCDF of the theoretical link achievable rate in the HPAV frequency band (a) and in the extended band 2-100 MHz (b).

Now, we focus on the HPAV frequency band 2-28 MHz and in the extended band 2-100 MHz. In Fig. 12, we show the CCDF of the achievable rate for the two BB frequency ranges of interest, for two different states of the vehicle. We note that PLC channels can convey high rate. At 70%, the theoretical achievable rate is in excess of 140 Mbps and up to 170 Mpbs in the HPAV band, depending on the vehicle state. The performances increases by up to 400% in the extended band. The analysis shows that there is margin to develop practical schemes that provide high reliability for the data rates of interest in vehicular applications. In this respect, an analysis of the performance that can be achieved by applying multicarrier (MC) and impulsive ultra wideband (I-UWB) modulation to in-car power line channels has been performed in [18].

VI. CONCLUSION

In this paper, we have presented the results of an entire PLC noise and channel measurement campaign that we have performed in a compact electrical car. We have set our focus on the noise caused by the electric and electronic components of the vehicle. We have demonstrated that the main noise sources are the DC/DC converter and the concatenated voltage generated by the high current that flows to the electric engines. We have derived an analytic model for the harmonic content of the NB PLC noise, and we have given an overview to the BB harmonic components. Furthermore, from measures, we have studied the potential data transmission performance in terms of theoretical achievable rate. We have considered both the NB spectrum, i.e., the Cenelec bands A, B, and C, and the BB spectrum. In the NB, the achievable data rate is in excess of 60 kbps and up to 300 kbps depending on the considered band and the vehicle state. In particular, performance decreases by up to 25% when the electric engines run under heavy load conditions. Conversely, the BB PLC channel can potentially convey high data rate due to the presence of lower noise. Thus, practical schemes that provide high speed and reliable communications can be developed in the BB case.

REFERENCES

[1] A. Schiffer, "Statistical channel and noise modeling of vehicular DC-lines for data communication," in *Proc. IEEE Veh. Technol. Conf. (VTC)*, vol. 1, pp. 158-162, 2000.

[2] P. A. J. van Rensburg, and H. C. Ferreira, "Automotive Power-Line Communications: Favourable Topology for Future Automotive Electronic Trends," in *Proc. IEEE Int. Symp. on Power Line Commun. and Its Appl. (ISPLC)*, pp. 103-108, 2003.

[3] P. A. J. van Rensburg, H. C. Ferreira, and A. J. Snyders, "An experimental setup for in-circuit optimization of broadband automotive power-line communications," in *Proc. IEEE Int. Symp. on Power Line Commun. and Its Appl. (ISPLC)*, pp. 322-325, 2005.

[4] T. Huck, J. Schirmer, and K. Dostert, "Tutorial about the Implementation of a Vehicular High Speed Communication System," in *Proc. IEEE Int. Symp. on Power Line Commun. and Its Appl. (ISPLC)*, pp. 162-166, 2005.

[5] M. O. Carrion, M. Lienard, and P. Degauque, "Communication over Vehicular DC Lines: Propagation Channel Characteristics," in *Proc. IEEE Int. Symp. on Power Line Commun. and Its Appl. (ISPLC)*, pp.2-5, 2006.

[6] W. Gouret, F. Nouvel, and G. El-Zein, "Powerline Communication on Automotive Network," in *Proc. IEEE Veh. Technol. Conf. (VTC)*, pp. 2545-2549, 2007.

[7] V. Degardin, M. Lienard, P. Degauque, and P. Laly, "Performances of the HomePlug PHY Layer in the Context of In-Vehicle Powerline Communications," in *Proc. IEEE Int. Symp. on Power Line Commun. and Its Appl. (ISPLC)*, pp. 93-97, 2007.

[8] M. Lienard, M. Carrion, V. Degardin, and V. Degauque, "Modeling and Analysis of In-Vehicle Power Line Communication Channels," *IEEE Trans. Veh. Technol.*, vol. 57, no. 2, pp. 670-679, 2008.

[9] V. Degardin, M. Lienard, P. Degauque, E. Simon, and P. Laly, "Impulsive Noise Characterization of In-Vehicle Power Line," *IEEE Trans. Electromagn. Compat.*, vol. 50, no. 4, pp. 861-868, 2008.

[10] M. Mohammadi, L. Lampe, M. Lok, S. Mirabbasi, M. Mirvakili, R. Rosales, and P. van Veen, "Measurement Study and Transmission for In-Vehicle Power Line Communication," in *Proc. IEEE Int. Symp. on Power Line Commun. and Its Appl. (ISPLC)*, pp. 73-78, 2009.

[11] A. B. Vallejo-Mora, J. J. Sáchez-Martínez, F. J. Cañete, J. A. Cortés, and L. Díez, "Characterization and Evaluation of In-Vehicle Power Line Channels," in *Proc. IEEE Global Telecommun. Conf.*, pp.1-5, 2010.

[12] J. A. Cortés, M. Cerdá, L. Díez, F. J. Cañete, "Analysis of the periodic noise on in-vehicle broadband power line channels," in *Proc. IEEE Int. Symp. on Power Line Commun. and Its Appl. (ISPLC)*, pp. 334-339, 2012.

[13] S. Barmada, M. Raugi, M. Tucci, and T. Zheng, "Power Line Communication in a full electric vehicle: Measurements, modelling and analysis," in *Proc. IEEE Int. Symp. on Power Line Commun. and Its Appl. (ISPLC)*, pp. 331-336, 2010.

[14] N. Taherinejad, R. Rosales, L. Lampe, and S. Mirabbasi, "Channel characterization for power line communication in a hybrid electric vehicle," in *Proc. IEEE Int. Symp. on Power Line Commun. and Its Appl. (ISPLC)*, pp. 328-333, 2012.

[15] http://www.estrima.com.

[16] HomePlug AV white paper [Online]. Available: http://www.homeplug.org.

[17] ERDF, *PLC G3 Physical Layer Specification*. [Online]. Available: http://www.maximintegrated.com/products/powerline/pdfs/G3-PLC-Physical-Layer-Specification.pdf

[18] M. Antoniali, M. Girotto, and A. M. Tonello, "In-car Power Line Communications: Advanced Transmission Techniques," *International Journal of Automotive Technology*, in press.